Available online at www.sciencedirect.com
ScienceDirect
Journal of Sound and Vibration 310 (2008) 352–365
JOURNAL OF SOUND AND VIBRATION
www.elsevier.com/locate/jsvi

Preview control of random response of a half-car vehicle model traversing rough road

L.V.V. Gopala Rao, S. Narayanan*

Machine Design Section, Department of Mechanical Engineering, Indian Institute of Technology Madras, Chennai 600 036, India

Received 27 February 2006; received in revised form 30 July 2007; accepted 2 August 2007
Available online 27 September 2007

Abstract

The semi-active control of response of a four degree-of-freedom (dof) half-car model traversing at constant velocity a random road with look ahead preview is considered. The suspension spring is assumed to be hysteretic nonlinear and modelled by the Bouc–Wen model. The statistical linearization technique is used to derive an equivalent linear model. The response of the vehicle is optimized with respect to suspension stroke, road holding and control force. The rms values of the suspension stroke, road holding and control forces are computed using the spectral decomposition method. The results for the equivalent linear model obtained by the spectral decomposition method are verified using Monte Carlo simulation. It is shown that the preview control results in a better vehicle performance.

1. Introduction

In recent years, much research has been carried out in the design of active and semi-active suspensions of vehicles for better vehicle response. The conventional passive suspension system of road vehicles consists of a combination of springs and dampers. The characteristics of such suspension elements cannot be altered by design during operation. In active vehicle suspension systems the external excitation is counteracted with the generation of a control force depending on the vehicle response through an actuator driven by an external energy source. However, difficulties in control hardware implementation, high cost and relatively less robustness restrict the use of active suspensions. The semi-active suspension system is an alternate to the active suspension system and these systems have been proposed by Karnopp et al. [1]. The semi-active suspension system can combine the advantages of the active suspension system while providing more robustness to the suspension performance. Usually in a semi-active suspension system, the actuator is replaced by a rapidly adjustable damper which acts in parallel with a spring.

Semi-active devices have been used in a variety of applications for vibration control in many areas such as in the control of building vibration due to earthquakes and wind forces [2], vehicles traversing rough roads [3–5]. The semi-active suspension performance can be improved using future information of the oncoming road input. Bender [6] was one of the first to propose a preview control scheme for a single degree-of-freedom (dof)

*Corresponding author. Tel.: +91 44 22 574 668; fax: +91 44 22 576 668.
E-mail address: narayans@iitm.ac.in (S. Narayanan).

0022-460X/$ - see front matter © 2007 Elsevier Ltd. All rights reserved.
doi:10.1016/j.jsv.2007.08.004

vehicle model which was also applied to the preview control of quarter car [7,8] and half-car vehicle models [9–11]. It was observed that the performance of the vehicle in all aspects can be improved with preview information. Most of the works concerning vehicular response control with preview of a half-car vehicle model hitherto has been confined to linear models.

Many authors have modeled the passive suspension elements with linear springs and dampers. However, the force deformation characteristics of vehicular suspension springs exhibit nonlinear behavior of the hysteretic type. Many types of hysteresis models have been proposed for the characterization of vehicle suspensions. Narayanan and Senthil [12] have considered the preview control of a two-dof vehicle model with nonlinear passive elements such as quadratic dampers and hysteretic stiffness elements. They modeled the hysteretic nature of these springs by the Bouc–Wen model [13].

The preview control problem involves both feed forward and feed back components. The feed forward component requires the preview information which is obtained using sensors and the feed back component requires the suspension system state variables information. Thompson et al. [14] have used the spectral decomposition method to solve preview control problems applied to vehicle suspensions.

The response of nonlinear systems to random excitation can be obtained using either approximate analytical or simulation techniques. Yadav and Nigam [15] have used simulation techniques to analyze the response behavior of nonlinear vehicle models. Analytical methods are preferred wherever possible, due to the large computational time involved in simulation techniques. The analytical methods include the perturbation, equivalent linearization and various closure techniques. The equivalent linearization technique is one of the most widely used techniques in the analysis of nonlinear systems subjected to random excitation [16,17].

In this paper, the preview control of the random response of a half-car vehicle model is investigated. The vehicle is modeled as a four dof half-car model with passive suspension elements consisting of a damper and hysteretic type nonlinear spring. The hysteretic nature of the suspension spring is modeled by a Bouc–Wen model which gives the relationship between the smooth hysteretic restoring force and relative displacement. The equivalent linearization method is used for obtaining the response of the vehicle. The vehicular response traversing a rough road with constant velocity is optimized using preview control minimizing a performance index which is a weighted sum of the front and rear suspension strokes, tyre deflections and control forces. The random road profile is modeled as the response of a linear first-order filter to white-noise excitation. The rms values of the front and rear suspension strokes, tyre deflections and control forces are computed using the spectral decomposition method.

2. Mathematical modeling

2.1. Theoretical formulation

The schematic of a half-car model with nonlinear suspension stiffness and look ahead preview is shown in Fig. 1. The nonlinearity of the suspension spring is assumed to be of hysteretic type and modeled using the Bouc–Wen model. The equations of motion of the half-car vehicle model can be expressed as

$$\begin{aligned} M\ddot{y}_c = {} & c_1(\dot{y}_1-\dot{y}_2)+\alpha_1k_1(y_1-y_2)-(1-\alpha_1)k_1z_f \\ & + c_2(\dot{y}_3-\dot{y}_4)+\alpha_2k_2(y_3-y_4)-(1-\alpha_2)k_2z_r+u_1+u_2, \end{aligned} \tag{1}$$

$$\begin{aligned} I\ddot{\theta} = {} & a[c_1(\dot{y}_1-\dot{y}_2)+\alpha_1k_1(y_1-y_2)-(1-\alpha_1)k_1z_f] \\ & - b[c_2(\dot{y}_3-\dot{y}_4)+\alpha_2k_2(y_3-y_4)-(1-\alpha_2)k_2z_r]+u_1a-u_2b, \end{aligned} \tag{2}$$

$$m_1\ddot{y}_1 = c_1(\dot{y}_2-\dot{y}_1)+\alpha_1k_1(y_2-y_1)-(1-\alpha_1)k_1z_f+k_{tf}(h_f-y_1)-u_1, \tag{3}$$

$$m_2\ddot{y}_3 = c_2(\dot{y}_4-\dot{y}_3)+\alpha_2k_2(y_4-y_3)-(1-\alpha_2)k_2z_r+k_{tr}(h_r-y_3)-u_2, \tag{4}$$

$$\ddot{y}_2 = [c_1(\dot{y}_1-\dot{y}_2)+\alpha_1k_1(y_1-y_2)-(1-\alpha_1)k_1z_f+u_1]\delta+[c_2(\dot{y}_3-\dot{y}_4)+\alpha_2k_2(y_3-y_4)-(1-\alpha_2)k_2z_r+u_2]\eta, \tag{5}$$

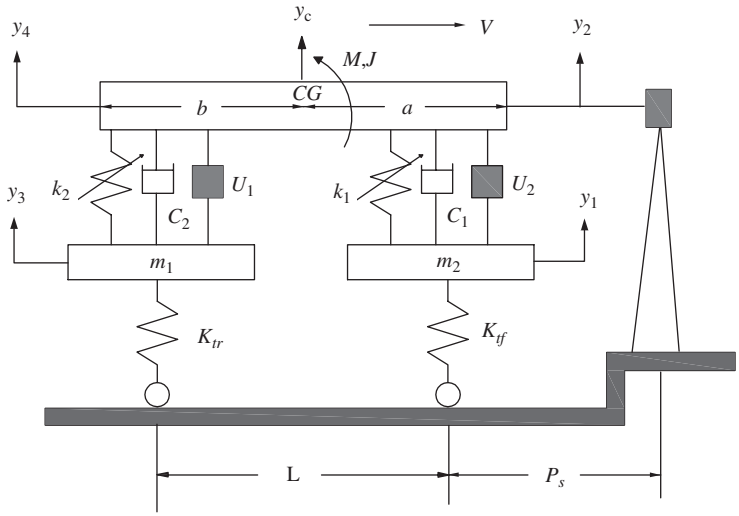

Fig. 1. Half-car model with preview control.

$$\ddot{y_4} = [c_1(\dot{y}_1 - \dot{y_2}) + \alpha_1 k_1(y_1 - y_2) - (1-\alpha_1)k_1 z_f + u_1]\eta + [c_2(\dot{y}_3 - \dot{y_4}) + \alpha_2 k_2(y_3 - y_4) - (1-\alpha_2)k_2 z_r + u_2]\zeta, \tag{6}$$

where

$$\delta = 1/M + a^2/J, \quad \eta = 1/M - ab/J, \quad \zeta = 1/M + b^2/J, \tag{7}$$

$$y_2 = y_c + a\theta, \quad y_4 = y_c - b\theta, \tag{8}$$

where y_2 and y_4 are absolute displacements of the front and rear end of the vehicle body, y_1 and y_3 are absolute displacements of the front and rear unsprung masses m_1 and m_2, respectively, M is the sprung mass, I is the mass moment of inertia of the vehicle about a centroidal axis, c_1 and c_2 are front and rear suspension damping coefficients, α_1 and k_1 are the front hysteretic suspension spring parameters, α_2 and k_2 are the rear hysteretic suspension spring parameters, k_{tf} is the front tyre stiffness, k_{tr} is the rear tyre stiffness, u_1 and u_2 are the front and rear control forces and the parameters z_f and z_r are the front and rear suspension hysteretic displacements, respectively. The hysteresis displacements are governed by the following equations as per the Bouc–Wen model:

$$\dot{z}_f = -\gamma_f|\dot{y}_2 - \dot{y_1}|z_f|z_f|^{n-1} - \beta_f|z_f|^n(\dot{y}_2 - \dot{y_1}) + A_f(\dot{y}_2 - \dot{y_1}), \tag{9}$$

$$\dot{z}_r = -\gamma_r|\dot{y}_4 - \dot{y_3}|z_r|z_r|^{n-1} - \beta_r|z_r|^n(\dot{y}_4 - \dot{y_3}) + A_r(\dot{y}_4 - \dot{y_3}), \tag{10}$$

where γ_f, β_f and A_f are the parameters of the front hysteretic suspension and γ_r, β_r, A_r are the rear hysteretic suspension parameters. These parameters control the shape of the hysteresis loop. The parameter n determines the smoothness of the force–displacement curve. Using the equivalent linearization technique [18] Eqs. (9) and (10) can be represented in equivalent linear form as

$$\dot{z}_f = C_{hf}(\dot{y}_2 - \dot{y_1}) + K_{hf} z_f, \tag{11}$$

$$\dot{z}_r = C_{hr}(\dot{y}_4 - \dot{y_3}) + K_{hr} z_r, \tag{12}$$

where C_{hf} and K_{hf} are the equivalent damping coefficient and stiffness, which are obtained by minimizing the mean square of the error between Eqs. (9) and (11). These values are given by

$$C_{hf} = -\gamma g_{1f} - \beta g_{2f} + A_{hf}, \tag{13}$$

$$K_{hf} = -\gamma g_{3f} - \beta g_{4f}, \tag{14}$$

$$g_{1f} = \frac{\sigma_{z_f}^n}{\pi}\Gamma\left(\frac{n+2}{2}\right)2^{n/2}F_s, \tag{15}$$

$$g_{2f} = \frac{\sigma_{z_f}^n}{\sqrt{\pi}}\Gamma\left(\frac{n+1}{2}\right)2^{n/2}, \tag{16}$$

$$g_{3f} = \frac{n\sigma_{(\dot{y}_2-\dot{y}_1)}\sigma_{z_f}^{n-1}}{\pi}\Gamma\left(\frac{n+2}{2}\right)2^{n/2}\left[2(1-\rho^2_{(\dot{y}_2-\dot{y}_1)z_f})^{(n+1)/2} + \rho_{(\dot{y}_2-\dot{y}_1)z_f}F_s\right], \tag{17}$$

$$g_{4f} = \frac{n\rho_{(\dot{y}_2-\dot{y}_1)z_f}\sigma_{(\dot{y}_2-\dot{y}_1)}\sigma_{z_f}^{n-1}}{\sqrt{\pi}}\Gamma\left(\frac{n+1}{2}\right)2^{n/2}, \tag{18}$$

where

$$F_s = 2\int_l^{\pi/2}\sin^n\theta\,\mathrm{d}\theta,$$

$$l = \tan^{-1}\left(\frac{\sqrt{1-\rho^2_{(\dot{y}_2-\dot{y}_1)z_f}}}{\rho_{(\dot{y}_2-\dot{y}_1)z_f}}\right),$$

$$\rho_{(\dot{y}_2-\dot{y}_1)z_f} = \frac{E[(\dot{y}_2-\dot{y}_1)z_f]}{\sigma_{(\dot{y}_2-\dot{y}_1)}\sigma_{z_f}},$$

where $\sigma_{(\dot{y}_2-\dot{y}_1)}$ is the standard deviation of the front suspension relative velocity. $\sigma_{z_{(\cdot)}}$ is the standard deviation of the Bouc–Wen model hysteretic displacement, $\rho_{(\cdot)}$ is the correlation coefficient between relative velocity and hysteretic displacement and $\Gamma(\cdot)$ is the gamma function.

Similarly Eq. (10) can also be written in the approximated linear form as Eq. (12), the subscript r referring to the rear wheel and the parameters of Eq. (10) are defined by equations similar to Eqs. (13)–(18).

3. State space formulation and control scheme

Eqs. (11) and (12) can be written in state space form as

$$\dot{z} = Az + Gu + D\dot{w}, \tag{19}$$

where

$$z = [z_1 \quad z_2 \quad z_3 \quad z_4 \quad z_5 \quad z_6 \quad z_7 \quad z_8 \quad z_f \quad z_r]^{\mathrm{T}} \tag{20}$$

with

$$z_1 = y_1 - h_f; \quad z_2 = y_2 - y_1; \quad z_3 = y_5; \quad z_4 = y_6$$

$$z_5 = y_3 - h_r; \quad z_6 = y_4 - y_3; \quad z_7 = y_7; \quad z_8 = y_8$$

$$\dot{y_1} = y_5; \quad \dot{y_2} = y_6; \quad \dot{y_3} = y_7; \quad \dot{y_4} = y_8.$$

A, G and D are system matrix, control distribution matrix and excitation distribution matrix, respectively and z is the state variable vector, u is the control vector and w is the disturbance vector. These

are given by

$$A=\begin{bmatrix}
0 & 0 & 1 & 0 & 0 & 0 & 0 & 0 & 0 & 0\\
0 & 0 & -1 & 1 & 0 & 0 & 0 & 0 & 0 & 0\\
\dfrac{-k_{\mathrm{tf}}}{m_1} & \dfrac{\alpha_1 k_1}{m_1} & \dfrac{-c_1}{m_1} & \dfrac{c_1}{m_1} & 0 & 0 & 0 & 0 & \dfrac{(1-\alpha_1)k_1}{m_1} & 0\\
0 & -\delta\alpha_1 k_1 & \delta c_1 & -\delta c_1 & 0 & -\eta\alpha_2 k_2 & \eta c_2 & -\eta c_2 & \delta(1-\alpha_1)k_1 & \eta(1-\alpha_2)k_2\\
0 & 0 & 0 & 0 & 0 & 0 & 1 & 0 & 0 & 0\\
0 & 0 & 0 & 0 & 0 & 0 & -1 & 1 & 0 & 0\\
0 & 0 & 0 & 0 & \dfrac{-k_{\mathrm{tr}}}{m_2} & \dfrac{\alpha_2 k_2}{m_2} & \dfrac{-c_2}{m_2} & \dfrac{c_2}{m_2} & 0 & \dfrac{(1-\alpha_2)k_2}{m_2}\\
0 & -\eta\alpha_1 k_1 & \eta c_1 & -\eta c_1 & 0 & -\zeta\alpha_2 k_2 & \zeta c_2 & -\zeta c_2 & \eta(1-\alpha_1)k_1 & \zeta(1-\alpha_2)k_2\\
0 & 0 & c_f & -c_f & 0 & 0 & 0 & 0 & -k_f & 0\\
0 & 0 & 0 & 0 & 0 & 0 & c_r & -c_r & 0 & -k_r
\end{bmatrix}, \tag{21}$$

$$G=\begin{bmatrix}
0 & 0 & \dfrac{-1}{m_1} & \delta & 0 & 0 & 0 & \eta & 0 & 0\\
0 & 0 & 0 & \eta & 0 & 0 & \dfrac{-1}{m_2} & \zeta & 0 & 0
\end{bmatrix}^{\mathrm{T}}, \tag{22}$$

$$D=[d_1\ \ d_2]^{\mathrm{T}}, \tag{23}$$

$$d_1=[-1\ \ 0\ \ 0\ \ 0\ \ 0\ \ 0\ \ 0\ \ 0\ \ 0\ \ 0]^{\mathrm{T}},$$

$$d_2=[0\ \ 0\ \ 0\ \ 0\ \ -1\ \ 0\ \ 0\ \ 0\ \ 0\ \ 0]^{\mathrm{T}},$$

$$\dot{w}=[\dot{h}_f\ \ \dot{h}_r]^{\mathrm{T}},$$

$$h_f(t)=U(t-T_1),$$

$$h_r(t)=U(t-T_2),$$

where h_f and h_r are unit step road inputs at the front and rear wheels, respectively.

The displacement power spectral density (psd) of the road profile is given by [14]

$$\Phi(\omega)=\frac{cV}{\omega^2}, \tag{24}$$

where c is the road roughness constant, ω is the angular frequency and V is the vehicle forward velocity. Thompson and Davis [19] have given a relation, for linear systems, between the integral squared values of the response to the unit step input and the mean-squared value of output to random excitation. Using this relation corresponding to the unit step input the rms values of the response of the half-car model can be obtained. Henceforth, in further discussion the state vector $z(t)$ corresponds to the response to the step excitation considered equivalent to the random road input given by the psd of Eq. (24). The rms values of the state vector $z(t)$ and the control force $u(t)$ are given by [14]

$$\langle z(t)z^{\mathrm{T}}(t)\rangle = 2\pi cV\int_0^\infty z(t)z^{\mathrm{T}}(t)\,\mathrm{d}t, \tag{25}$$

$$\langle u(t)u^{\mathrm{T}}(t)\rangle = 2\pi cV\int_0^\infty u(t)u^{\mathrm{T}}(t)\,\mathrm{d}t. \tag{26}$$

3.1. Optimal preview control law

The optimal suspension is designed using the optimal control law which is derived by minimizing the weighted sum of the front and rear tyre deflections, suspension strokes and the control forces. The performance index J is given by

$$J = \int_0^\infty [\rho_1 u_1^2 + \rho_2 u_2^2 + q_1(y_1 - h_f)^2 + q_2(y_1 - y_2)^2 + q_3(y_3 - h_r)^2 + q_4(y_3 - y_4)^2]\,\mathrm{d}t, \tag{27}$$

where $\rho_1, \rho_2, q_1, q_2, q_3$ and q_4 are appropriate weighting factors. The performance index can be written as

$$J = \int_0^\infty (zQz^{\mathrm{T}} + uBu^{\mathrm{T}})\,\mathrm{d}t, \tag{28}$$

where

$$Q = \mathrm{diag}[q_1 \;\; q_2 \;\; 0 \;\; 0 \;\; q_3 \;\; q_4 \;\; 0 \;\; 0 \;\; 0 \;\; 0],$$

$$B = \mathrm{diag}[\rho_1 \;\; \rho_2].$$

The optimal preview control force is given by

$$u(t) = F_b z(t) + F_f r(t), \tag{29}$$

where

$$F_b = -B^{-1} G^{\mathrm{T}} S, \tag{30}$$

$$F_f = -B^{-1} G^{\mathrm{T}} \tag{31}$$

and S is the positive definite solution of the matrix Riccati equation given by

$$A^{\mathrm{T}} S + SA - SGB^{-1} GS + Q = 0. \tag{32}$$

Substituting Eqs. (29)–(31) in Eq. (19) we get

$$\dot{z} = A_c z - GB^{-1} G^{\mathrm{T}} r(t) + D\dot{w}, \tag{33}$$

$$A_c = A - GB^{-1} G^{\mathrm{T}} S. \tag{34}$$

In Eq. (29), $r(t)$ is a vector governed by

$$\dot{r}(t) + A_c r + SD\dot{w} = 0. \tag{35}$$

3.2. Spectral decomposition

Eqs. (33) and (35) can be written in composite form as

$$\begin{bmatrix} \dot{z} \\ \dot{r} \end{bmatrix} = \begin{bmatrix} A_c & -GB^{-1} G^{\mathrm{T}} \\ 0 & -A_c^{\mathrm{T}} \end{bmatrix} \begin{bmatrix} z \\ r \end{bmatrix} + \begin{bmatrix} D \\ -SD \end{bmatrix} \dot{w}. \tag{36}$$

The above coupled equations can be changed to uncoupled equations by converting the system equations to a diagonal form. The eigenvalues and eigen vectors are determined as

$$\begin{bmatrix} A_c & -GB^{-1} G^{\mathrm{T}} \\ 0 & -A_c^{\mathrm{T}} \end{bmatrix} \begin{bmatrix} V_{11} & V_{12} \\ 0 & V_{22} \end{bmatrix} = \begin{bmatrix} V_{11} & V_{12} \\ 0 & V_{22} \end{bmatrix} \begin{bmatrix} \lambda & 0 \\ 0 & -\lambda \end{bmatrix}. \tag{37}$$

Using the above equation we can write the submatrix A_c in the spectral decomposition form as $V_{11}^{-1}A_cV_{11}=\lambda$. Let $V_{11}^{-1}=U_{11}$ and

$$\begin{bmatrix} x_a \\ x_b \end{bmatrix} = \begin{bmatrix} U_{11} & U_{12} \\ 0 & U_{22} \end{bmatrix} \begin{bmatrix} z \\ r \end{bmatrix} \tag{38}$$

by substituting Eq. (38) in Eq. (36) we obtain

$$\begin{bmatrix} \dot{x}_a \\ \dot{x}_b \end{bmatrix} = \begin{bmatrix} \lambda & 0 \\ 0 & \lambda \end{bmatrix} \begin{bmatrix} x_a \\ x_b \end{bmatrix} + \begin{bmatrix} U_{11} & U_{12} \\ 0 & U_{22} \end{bmatrix} \begin{bmatrix} D \\ -SD \end{bmatrix} \dot{w}. \tag{39}$$

Solution of Eq. (39) is obtained as

$$\begin{bmatrix} x_a \\ x_b \end{bmatrix} = \begin{bmatrix} e^{\lambda t} & 0 \\ 0 & -e^{\lambda t} \end{bmatrix} \left(\begin{bmatrix} x_{0a} \\ x_{0b} \end{bmatrix} + \begin{bmatrix} x_{1a} \\ x_{1b} \end{bmatrix} U(t-T_1) + \begin{bmatrix} x_{1a} \\ x_{1b} \end{bmatrix} U(t-T_1) \right), \tag{40}$$

where $U(t)$ is the unit step function.

4. Results and discussion

The half-car vehicle model with the following parameters is considered as an example.

$M=730\,\text{kg}$, $I=1230\,\text{kg m}^2$, $m_1=40\,\text{kg}$, $m_2=35.5\,\text{kg}$, $c_1=1290\,\text{Ns/m}$, $c_2=1620\,\text{Ns/m}$, $k_1=19960\,\text{N/m}$, $k_2=17500\,\text{N/m}$, $k_{\text{tf}}=175,500\,\text{N/m}$, $k_{\text{tr}}=175,500\,\text{N/m}$, $a=1.011\,\text{m}$, $b=1.803\,\text{m}$, $c=10^{-5}\,\text{m}$, $q_1=q_3=10$, $q_2=q_4=10$, $\rho_1=\rho_2=0.5\times10^{-8}$.

The Bouc–Wen model parameters are assumed to be

$A_f=A_r=1.5$, $\gamma_f=\gamma_r=0.5$, $\beta_f=\beta_r=0.5$, $\alpha_1=\alpha_2=0.2$.

4.1. Spectral decomposition

In the following the results obtained based on Eqs. (25) and (26) and the spectral decomposition method given in the previous section are presented and discussed.

In Fig. 2 the overall performance is plotted as a function of the preview distance for various velocities. It is seen from the figure that the overall performance improves with increasing preview distance but saturates beyond a particular preview distance. Thus there is a limiting preview distance beyond which the benefit of preview control saturates. This distance increases with increase in vehicle velocity.

Fig. 3 shows the rms front wheel deflection for different vehicle velocities as a function of preview distance. It is seen from the figure that the performance of the vehicle with respect to the front wheel vehicle deflection is improved with preview control. It is also observed that the performance saturates with increasing preview distance and beyond a particular distance the performance actually deteriorates indicating an optimum preview distance with respect to front wheel vehicle deflection.

Fig. 4 shows the rms values of the rear wheel deflection as a function of the vehicle velocity for different preview distances. It is observed that the preview control does not have significant influence on the rear wheel deflection as with preview and without preview the response is almost the same. This is natural to expect since the rear wheel is further away from the preview sensor and the effect of preview control tapers off with increase in preview distance.

Figs. 5 and 6 show the rms front wheel and rear wheel travel, respectively, as function of the vehicle velocity for different preview distances. It is seen that the performance with respect to front wheel travel significantly improves with increase in preview distance for all velocities while with respect to rear wheel travel, for lower velocities there is no improvement in performance, while at higher velocities the performance improves.

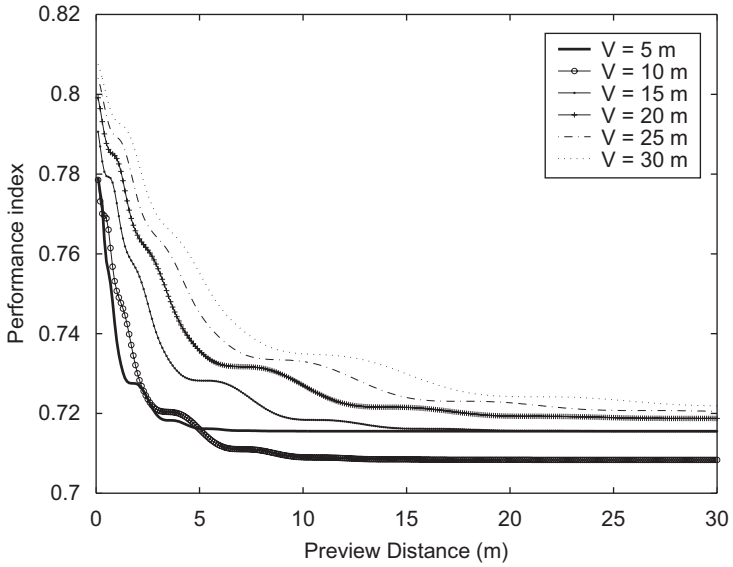

Fig. 2. Variation of the performance index with preview distance (P_d) for different velocities (V).

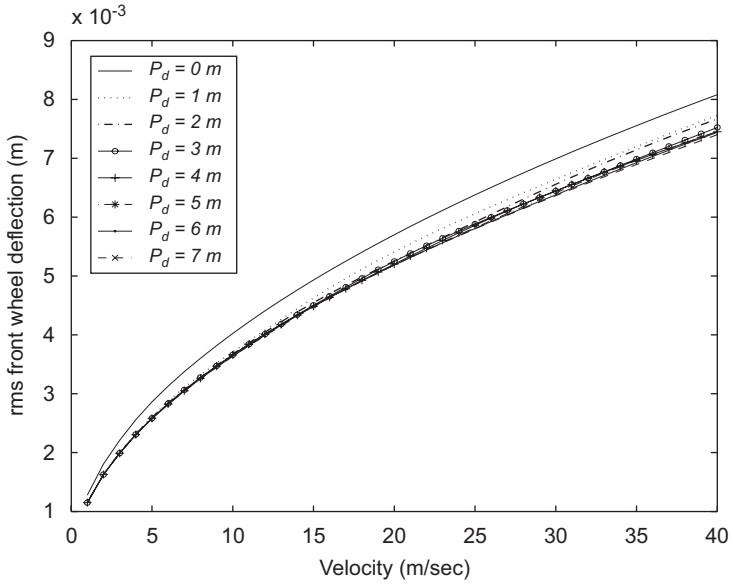

Fig. 3. Rms value of front tyre deflection for different preview distance (P_d).

Figs. 7 and 8 give the control effort required at the front and rear wheel, respectively, for different preview distances. It is obvious to expect the control effort required that will increase with the increase in preview distance. This is so, for both the front and the rear wheel, but this increase is more in respect of the front wheel as compared to the rear wheel.

4.2. Monte Carlo simulation

To verify the results obtained by the spectral decomposition method with the equivalent step excitation for the random road input and to verify the equivalent linearization technique Monte Carlo simulation studies are

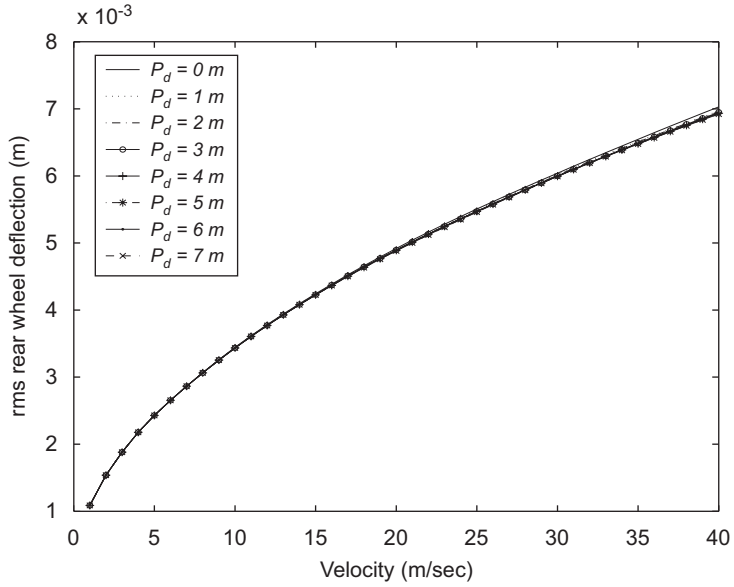

Fig. 4. Rms value of rear tyre deflection for different preview distances (P_d).

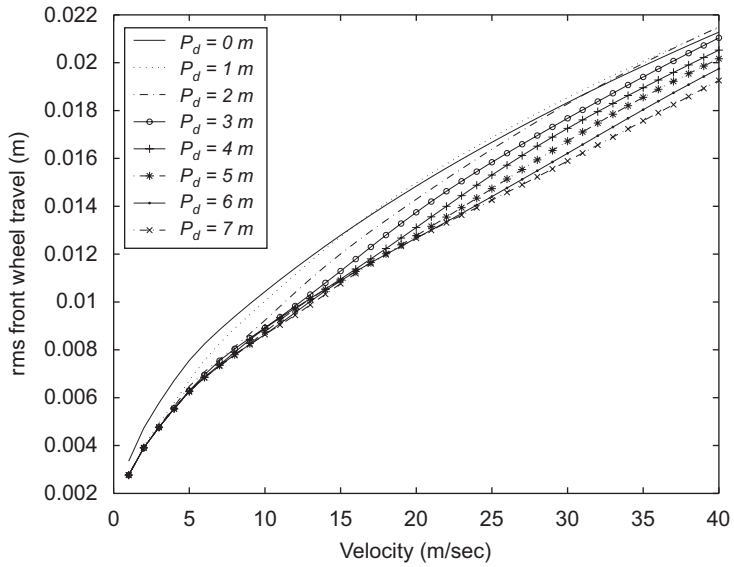

Fig. 5. Rms front wheel travel for different preview distances (P_d).

carried out. The method given by Shinozuka and Jan [20] is used to generate time histories of the front wheel road input $h_f(t)$ corresponding to the power spectral density function given in Eq. (24). The time histories are generated by the following series:

$$h_f(t) = \sqrt{2}\sum_{k=1}^{N}[S_h(\omega_k)\Delta\omega]^{\frac{1}{2}}\cos(\omega'_k + \phi_k), \tag{41}$$

where $S_h(\omega_k) = 2\Phi(\omega_k)$ is the one-sided power spectral density function at frequency ω_k, with $\omega_k = \omega_l + (k - \frac{1}{2})\Delta\omega,\ k = 1, 2, \ldots, N;\ \omega'_k = \omega_k + \delta\omega,\ k = 2, \ldots, N$ and $\Delta\omega = (\omega_u - \omega_l)/N$ with N being the number of equal intervals in which the frequency interval is divided. $\delta\omega$ is a small random frequency

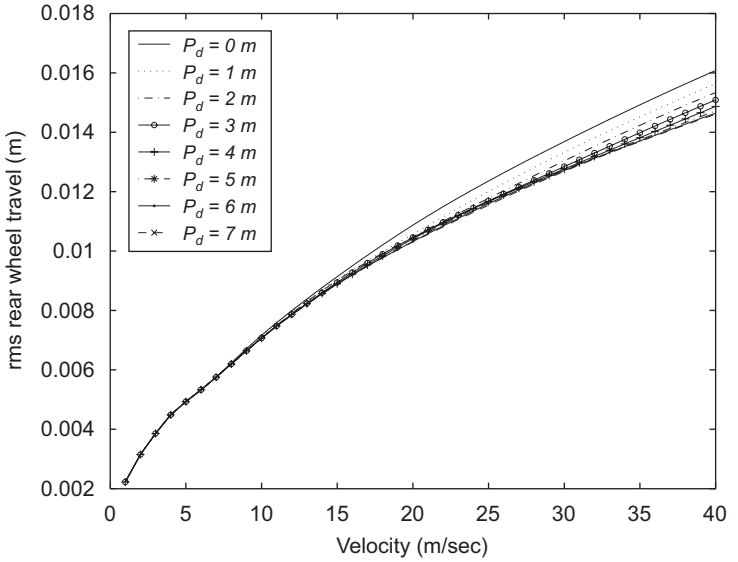

Fig. 6. Rms rear wheel travel for different preview distances (P_d).

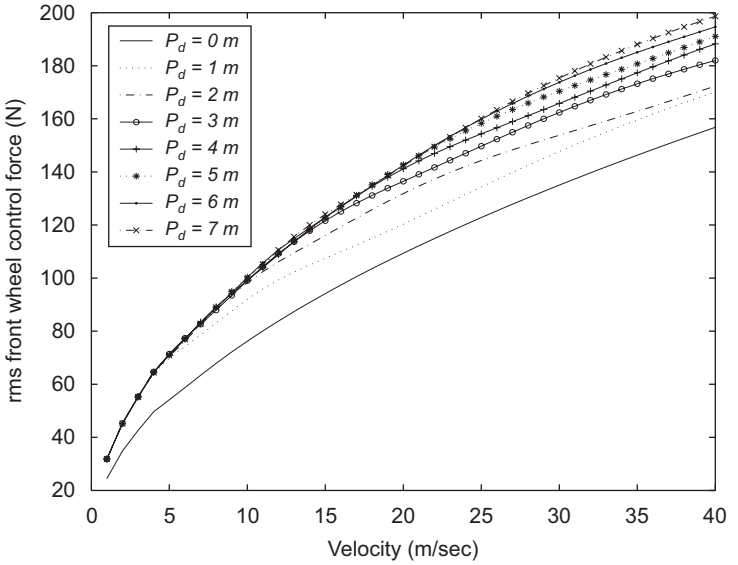

Fig. 7. Variation of the rms front wheel control force with velocity (P_d).

uniformly distributed between $-\Delta\omega'/2$ and $\Delta\omega'/2$ with $\Delta\omega' \ll \Delta\omega$ introduced to avoid the periodicity of the process which is simulated. ϕ_k's are independent random phase angles uniformly distributed in the interval 0 to 2π. ω_l and ω_u are respectively the lower and upper cut-off frequencies. The time history $h_f(t)$ is generated with $N = 1000$, $\omega_l = 0, \omega_u = 2\pi \times 100\,\text{rad/s}$, $\Delta\omega' = 0.05\,\Delta\omega$.

From the generated time history $h_f(t)$ the power spectral density function of the road input is obtained by using the MATLAB function 'psd' and is compared with the target power spectral density corresponding to Eq. (24) in Fig. 9 showing good agreement between the target psd and the simulated psd. The rear wheel road input $h_r(t)$ is obtained as the time delayed front wheel input $h_f(t - L/V)$. The equations of motion (3)–(8) with the nonlinear equations of the Bouc–Wen model equations (9) and (10) are numerically integrated with the control input given by Eq. (29). The control input $u(t)$ is the same as obtained by using Eqs. (30) to (35) for the equivalent linear model. The response statistics, rms front wheel travel, rms rear wheel travel, rms front tyre

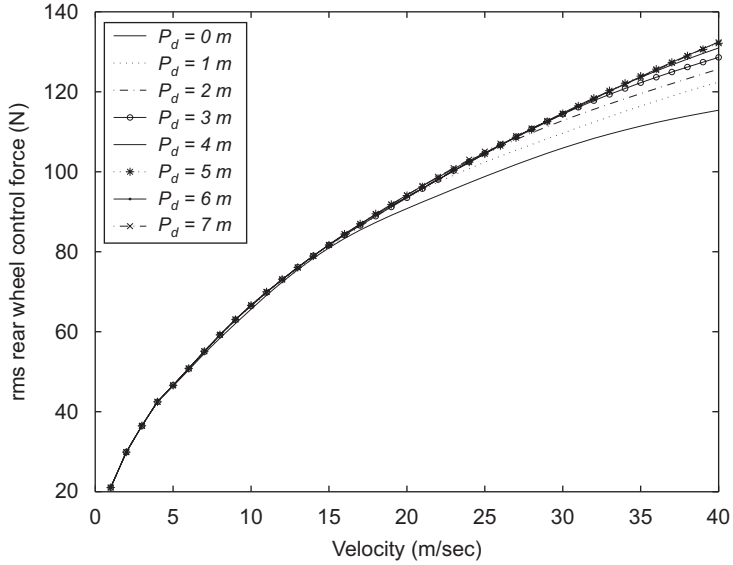

Fig. 8. Variation of the rms rear wheel control force with velocity (P_d).

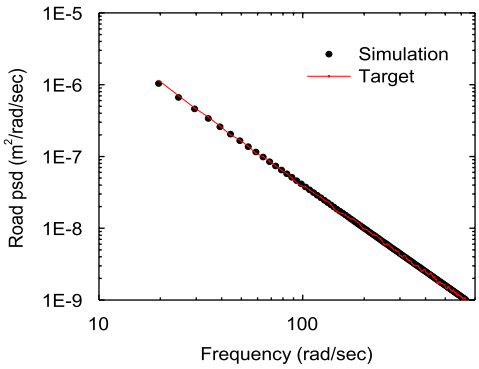

Fig. 9. Simulated and target psd of road profile.

deflection, rms rear wheel deflection are obtained from the generated time histories without preview control and with preview control for a preview distance of $P_d = 2$ m. These are plotted in Figs. 10–13 by the symbols '●' and '★' along with the results obtained by the equivalent linearization method. The agreement between the Monte Carlo simulated results and the results of the equivalent linearization method is very good validating not only the equivalent linearization technique but also the equivalent step input assumed for the random road excitation.

5. Conclusions

Active control of the response of a four degree of freedom half-car model with nonlinear suspension system which consists of dampers and hysteretic type nonlinear springs has been considered. The hysteretic nature of the suspension spring has been modeled by a Bouc–Wen model. The equivalent linearization method is used to obtain appropriate response statistics of the vehicle which is included in the control formulation. The random road excitation is equivalently modeled by an equivalent step input [14]. The spectral decomposition method is used to obtain the control gain matrix and the vehicle response.

The overall performance of the vehicle improves with preview control as compared to the performance without preview control. But the improvement with performance saturates beyond a preview distance.

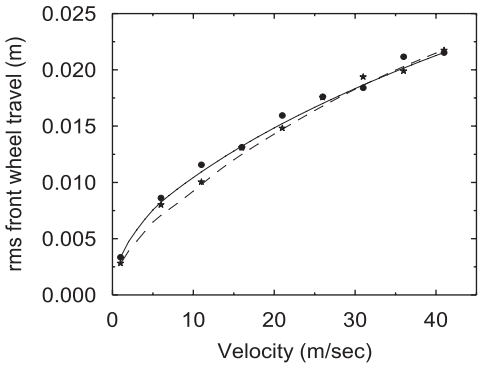

Fig. 10. Rms front wheel travel response with equivalent linearization ($P_d = 0$ m '–'; $P_d = 2$ m '– –') and simulation ($P_d = 0$ m '•'; $P_d = 2$ m '⋆').

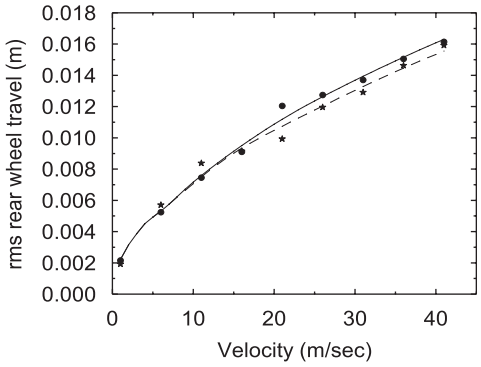

Fig. 11. Rms front wheel travel response with equivalent linearization ($P_d = 0$ m '–'; $P_d = 2$ m '– –') and simulation ($P_d = 0$ m '•'; $P_d = 2$ m '⋆').

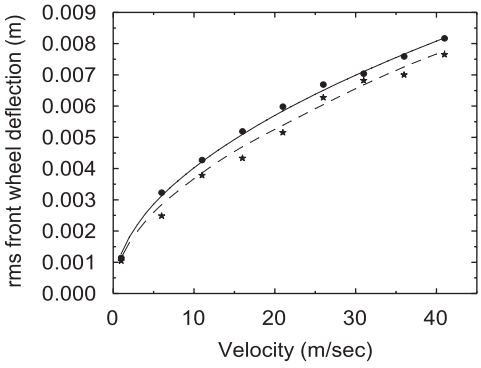

Fig. 12. Rms front wheel deflection response with equivalent linearization ($P_d = 0$ m '–'; $P_d = 2$ m '– –') and simulation ($P_d = 0$ m '•'; $P_d = 2$ m '⋆').

The performance with respect to individual vehicle responses such as front wheel tyre deflection, rear wheel tyre deflection, front wheel travel and rear wheel travel also improve with preview control. In these cases also the saturation in performance beyond a preview distance is observed. Hence, it is necessary to choose the preview distance judiciously as the control effort increases with increasing preview distance. It is also seen that the performance improvement with preview control is more perceptible in the case of front wheel responses than rear wheel responses. The rms front wheel travel performance improves with increasing preview distance

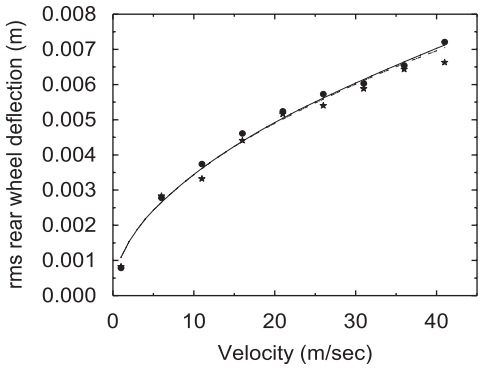

Fig. 13. Rms rear wheel deflection response with equivalent linearization ($P_d = 0$ m '–'; $P_d = 2$ m '– –') and simulation ($P_d = 0$ m '•'; $P_d = 2$ m '⋆').

with the improvement saturating as mentioned earlier. The rms rear wheel travel performance with preview control scheme is better than the zero-look ahead preview. But the rms rear wheel travel deflection performance is almost the same in both look ahead preview and zero-look ahead preview cases.

The equivalent linearization model and the equivalent step road input assumption are validated by Monte Carlo simulation by generating the road input compatable with the power spectral density function and numerically integrating the equations of motion with the nonlinear Bouc–Wen model.

References

[1] D. Karnopp, M.J. Crossby, R.A. Harwood, Vibration control using semiactive force generators, *Transactions of ASME, Journal of Engineering for Industry* 96 (1974) 619–626.
[2] W.Q. Zhu, M. Luo, L. Dong, Semi-active control of wind excited building structures using MR/ER dampers, *Probabilistic Engineering Mechanics* 19 (2004) 279–285.
[3] D.N.L. Horten, D.A. Crolla, Theoretical analysis of semiactive suspension fitted to an off-road vehicle, *Vehicle System Dynamics* 15 (1986) 351–372.
[4] M. Ahmadian, R.H. Marjoram, Effects of passive and semi-active suspensions on body and wheel hop, *SAE Transactions* 892487 (1989) 596–604.
[5] P. Holdmann, M. Holle, Possibilities to improve the ride and handling performance of delivery trucks by modern mechatronic systems, *JSAE Review* 20 (1999) 505–510.
[6] E.K. Bender, Optimal linear preview control with application to vehicle suspension, *Transactions of ASME, Journal of Basic Engineering* 90 (2) (1968) 213–221.
[7] A. Hac, Suspension optimization of a two dof vehicle model using stochastic optimal control technique, *Journal of Sound and Vibration* 100 (1985) 343–357.
[8] R.G.M. Huisman, F.E. Veldpaus, H.J.M. Voets, J.J. Kok, An optimal continuous time control strategy for active suspension with preview, *Vehicle System Dynamics* 22 (1993) 43–55.
[9] N. Louam, D.A. Wilson, R.S. Sharp, Optimal control of a vehicle suspension incorporating the time delay between front and rear wheel inputs, *Vehicle System Dynamics* 17 (1988) 317–336.
[10] S. Senthil, S. Narayanan, Stationary response of a four dof vehicle model with look ahead preview, *International Conference on Advances in Mechanical Engineering*, IISc Bangalore, Dec 20–22, 1995.
[11] J. Marzbanrad, G. Ahmadi, H. Zohar, Y. Hojjat, Stochastic optimal preview control of a vehicle suspension, *Journal of Sound and Vibration* 275 (2004) 973–990.
[12] S. Narayanan, S. Senthil, Stochastic optimal active control of a 2-dof quarter car model with non-linear passive suspension elements, *Journal of Sound and Vibration* 211 (3) (1998) 495–506.
[13] Y.K. Wen, Equivalent linearization for hysteretic systems under random excitation, *ASME Journal of Applied Mechanics* 47 (1980) 150–154.
[14] A.G. Thompson, B.R. Davis, Computation of the rms state variables and control forces in a half-car model with preview active suspension using spectral decomposition methods, *Journal of Sound and Vibration* 285 (3) (2005) 571–583.
[15] D. Yadav, N.C. Nigam, Ground induced nonstationary response of vehicles, *Journal of Sound and Vibration* 61 (1978) 117–126.
[16] T.T. Baber, Y.K. Wen, Random vibration of hysteretic degrading systems, *Transactions of ASCE, Journal of Engineering Division* 107 (1981) 1069–1087.
[17] A.X. Guo, Y.L. Xu, B. Wu, Seismic reliability of hysteretic structure with viscoelastic dampers, *Engineering Structures* 24 (2002) 373–383.

[18] J.E. Hurtado, A.H. Barbat, Equivalent linearization of the Bouc–Wen hysteretic model, *Engineering Structures* 24 (2002) 373–383.
[19] A.G. Thompson, C.E.M. Pearce, RMS values for force, stroke and deflection in a quarter-car model active suspension with preview, *Vehicle System Dynamics* 39 (1) (2003) 57–75.
[20] M. Shinozuka, C.M. Jan, Digital simulation of random process and its applications, *Journal of Sound and Vibration* 25 (1) (1972) 111–128.